

Supporting Information

Simulation-guided engineering of an enzyme-powered three dimensional DNA nanomachine for discriminating single nucleotide variants

Yongya Li,^{a,#} Alex Guan Wang,^{a,#} Sean D. Mason,^a Xiaolong Yang,^a Zechen Yu,^a Yanan Tang,^{a,b}
Feng Li^{a,b,*}

^aDepartment of Chemistry, Centre for Biotechnology, Brock University, St. Catharines, Ontario, Canada, L2S 3A1

^bCollege of Chemistry, Sichuan University, Chengdu, Sichuan, China, 610065

*Corresponding authors.

fli@brocku.ca

Y. Li and A. G. Wang contributed equally to this work

Table of Content:

S1. Experimental Section.....	2
S2. Bimolecular Model and Simulation of the Toehold-Exchange Reaction.....	5
S3. Two-Step Reaction Model and Simulation of the Non-Covalent DNA Catalysis.....	9
S4. Prediction of the Sequence Selectivity Using $\Delta\Delta G^\circ$	14
S5. Discrimination of SNV in Complicated Sample Matrix Using Catalytic 3DDN.....	15
S6. Long-Term Stability of the 3DDN System.....	16

S1. Experimental Section

Materials and Reagents. Solutions of 20-nm gold nanoparticles (AuNPs), TWEEN20, dithiothreitol (DTT), sodium chloride (NaCl), magnesium chloride hexahydrate (MgCl₂·6H₂O), and 100 × Tris-EDTA (TE) buffer were purchased from Sigma (Oakville, ON, Canada). Nicking endonuclease (Nb.BvCI) and 10 × CutSmart Buffer were purchased from New England Biolabs Ltd. (Whitby, ON, Canada). NANOpure H₂O (> 18.0 MΩ), purified using an Ultrapure Mili-Q water system, was used for all experiments. All DNA samples were purchased from Integrated DNA Technologies (Coralville, IA) and purified using high-performance liquid chromatography. The DNA sequences and modifications are listed in Table S1.

Table S1. DNA sequences and modifications.

DNA name		Sequences
DNA probes for constructing the 3D DNA Nanomachine	D (r = 10 nt)	5'-SH-T-50-T-ATT CAT GGG CCA <u>GAACA CCTCAGC</u> -3'-3'
	D (r = 5 nt)	5'-SH-T-50-T-ATT CAT GGG CCA <u>CCTCAGC</u> -3'-3'
	SR	5'-SH- T-10-T- GC*TGA GGAT-FAM-3'(*cleavage site)
	P (r = 10 nt)	5'- <u>TGAGG TG TTC</u> TGG CCC ATG AAT TGGC TCA <u>GCT</u> -3'
	P (r = 5 nt)	5'- <u>TGAGG</u> TGG CCC ATG AAT TGGC TCA <u>GCT</u> -3'
	F	5'- ATT CAT GGG CCA <u>GAACA CCTCA</u> -3'
Target DNA	WT	5'- AGC TGA GCCA ATT CAT GGG CCA-3'
	SNV19A	5'- AGC TGA GCCA ATT CAT GGA CCA-3'
	SNV19T	5'- AGC TGA GCCA ATT CAT GGT CCA-3'
	SNV19C	5'- AGC TGA GCCA ATT CAT GGC CCA-3'
	SNV12A	5'- AGC TGA GCCA AAT CAT GGG CCA-3'
	SNV12G	5'- AGC TGA GCCA AGT CAT GGG CCA-3'
	SNV12C	5'- AGC TGA GCCA ACT CAT GGG CCA-3'
	SNV7A	5'- AGC TGA ACCA ATT CAT GGG CCA-3'
	SNV7C	5'- AGC TGA CCA ATT CAT GGG CCA-3'
	SNV7T	5'- AGC TGA TCCA ATT CAT GGG CCA-3'

Preparation of the 3D DNA Nanomachine. The 3D DNA nanomachine was prepared by co-conjugating thiolated DNA probes onto the 20-nm AuNPs according to our previously established protocol. Briefly, 2.5 μM DNA walker (D) was first hybridized with equal amounts of the protecting DNA (P) through an annealing process. The obtained DP duplex was then mixed with signal reporter (R) at a ratio of 1 to 20. A 20 μL solution of this mixture containing 2.5 μM DP and 50 μM R was mixed with 1 mL of 1 nM AuNPs. This mixture was incubated at room temperature for 12 hrs and then was slowly mixed with 20 μL of 3 M NaCl solution, followed by 10 s of sonication. This salt aging process was repeated five times with a 1 h interval to maximize the density of oligonucleotide on AuNPs. The solution was then incubated for another 24 hrs. After incubation, the solution was centrifuged at 13,500 rpm for 30 min to separate the DNA-AuNP from the unreacted reagents. The DNA-AuNPs were then washed three times with $1 \times$ TE buffer (pH 7.4) containing 0.01% TWEEN 20 and finally redispersed in TE buffer.

Characterization of the 3D DNA Nanomachine. UV-vis spectrometry was used to characterize the quality of each DNA-AuNP solution and determine the concentration of the device. Typically, a maximum absorbance value of each DNA-AuNP solution was measured and compared to that of the unconjugated AuNP, whose concentration was provided by the vendor (1.16 nM). A red shift of 4-6 nm of the maximum absorbance could be observed upon the conjugation of DNA to AuNPs. The coverage of R oligonucleotides on each AuNP was then determined by releasing FAM-labeled R from AuNP using 20 mM DTT and measuring fluorescence of the FAM. Fluorescence was measured using a multimode microplate reader (SpectroMax i3, Molecular Devices), and R coverage was quantified by using FAM-labeled R as external standards. The coverage of DP on each AuNP was then estimated according to the R coverage and initial ratio between DP and R.

Detection of WT and SNV Targets Using the 3D DNA Nanomachine. For a typical reaction, a mixture containing 100 pM 3D device and varying concentrations of target DNA (WT or SNVs) were incubated at 37 $^{\circ}\text{C}$ for 10 min. Nicking endonuclease (20 U) was then added to each mixture to initiate the 3D walking. Immediately after the addition of the enzyme, fluorescence was measured every 1 min using a multimode microplate reader with an excitation/emission wavelength of 485/535 nm. To enhance the analytical performance of the 3DDN via noncovalent catalysis, the same protocol was used

for target analyses except that 10 nM fuel molecules (F) were added to the mixture of target and DNA nanomachine and followed by incubation at 37 °C for 1 hour before adding the nicking enzyme.

Characterization of non-covalent DNA catalysis using polyacrylamide gel electrophoresis (PAGE).

A reaction mixture containing 1 μM DP, 2 μM F, and 500 nM T (WT or SNV19A) was incubated at 37 °C for 1 hr. Reaction mixtures were then loaded onto 12% PAGE gel and a voltage of 110 V was applied. After electrophoresis, the gel was stained with Ethidium Bromide and imaged using Gel Doc XR+ Imager System (BioRad).

S2. Bimolecular Model and Simulation of the Toehold-Exchange Reaction

Determination of thermodynamic parameters using NuPACK. Standard Gibbs free energies for all DNA probes were estimated using NuPACK. The temperature and saline condition were set to be 37 °C, 100 mM Na⁺, and 10 mM Mg²⁺, which is consistent with our experimental conditions. The standard Gibbs free energy for the toehold-exchange between target (T) and DP was calculated using the following equation: $\Delta G^0_{\text{rxn}} = \Delta G^0_{\text{TP}} + \Delta G^0_{\text{D}} - \Delta G^0_{\text{DP}} - \Delta G^0_{\text{T}}$, and detailed in Table S2 (with forward toehold $f = 10$ nt) and Table S3 ($f = 9$ nt). The $\Delta\Delta G^0$ was then calculated according to the equation: $\Delta\Delta G^0 = \Delta G^0_{\text{rxn}}(\text{SNV}) - \Delta G^0_{\text{rxn}}(\text{WT})$, and detailed in Table S4.

Table S2. Thermodynamic parameters of the enzyme-powered 3D DNA nanomachine for the detection of a wild-type (WT) target and a SNV (SNV19A) target with forward toehold f fixed at 10 nt and reverse toehold r varying from 5 nt to 11 nt.

Reverse toehold r	$\Delta G^0(\text{TP})$ Kcal/mol (WT)	$\Delta G^0(\text{TP})$ Kcal/mol (SNV19A)	$\Delta G^0(\text{D})$ Kcal/mol	$\Delta G^0(\text{DP})$ Kcal/mol	$\Delta G^0(\text{T})$ Kcal/mol (WT)	$\Delta G^0(\text{T})$ Kcal/mol (SNV19A)	ΔG^0_{rxn} Kcal/mol (WT)	ΔG^0_{rxn} Kcal/mol (SNV19A)
5	-29.95	-24.69	-0.28	-23.38	-1.56	-2.04	-5.29	+0.45
6	-29.95	-24.69	-0.48	-25.37	-1.56	-2.04	-3.5	+2.24
7	-29.95	-24.69	-0.43	-25.77	-1.56	-2.04	-3.05	+2.69
8	-29.95	-24.69	0	-26.67	-1.56	-2.04	-1.72	+4.02
9	-29.95	-24.69	-1.52	-28.42	-1.56	-2.04	-1.49	+4.25
10	-29.95	-24.69	0	-29.37	-1.56	-2.04	+0.98	+6.72
11	-29.95	-24.69	-1.22	-31.11	-1.56	-2.04	+1.5	+7.24

Table S3. Thermodynamic parameters of the enzyme-powered 3D DNA nanomachine for the detection of a wild-type (WT) target and a SNV (SNV19A) target with forward toehold f fixed at 9 nt and reverse toehold r varying from 5 nt to 11 nt.

Reverse toehold r	$\Delta G^0(\text{TP})$ kcal/mol (WT)	$\Delta G^0(\text{TP})$ kcal/mol (SNV19A)	$\Delta G^0(\text{D})$ kcal/mol	$\Delta G^0(\text{DP})$ kcal/mol	$\Delta G^0(\text{T})$ kcal/mol (WT)	$\Delta G^0(\text{T})$ kcal/mol (SNV19A)	ΔG^0_{rxn} kcal/mol (WT)	ΔG^0_{rxn} kcal/mol (SNV19A)
5	-29.4	-24.13	-0.28	-23.38	-1.56	-2.04	-4.74	+1.01
6	-29.4	-24.13	-0.48	-25.37	-1.56	-2.04	-2.95	+2.8
7	-29.4	-24.13	-0.43	-25.77	-1.56	-2.04	-2.5	+3.25
8	-29.4	-24.13	0	-26.67	-1.56	-2.04	-1.17	+4.58
9	-29.4	-24.13	-1.52	-28.42	-1.56	-2.04	-0.94	+4.81
10	-29.4	-24.13	0	-29.37	-1.56	-2.04	+1.53	+7.28
11	-29.95	-24.69	-1.22	-31.11	-1.56	-2.04	+2.05	+7.8

Table S4. Thermodynamics of single-base changes.

Target	ΔG^0_{rxn} kcal/mol	$\Delta\Delta G^0$ kcal/mol
WT	+0.98	0
SNV19C	+8.42	+7.44
SNV19A	+6.72	+5.74
SNV19T	+6.47	+5.49
SNV12A	+3.98	+3.00
SNV12G	+2.92	+1.94
SNV12C	+4.41	+3.43
SNV7C	+8.30	+7.32
SNV7A	+5.99	+5.01
SNV7T	+5.61	+4.63

Bimolecular Model of the Toehold-Exchange. A typical toehold exchange reaction between T and DP can be written as: $T + DP \rightleftharpoons TP + D$, with a standard Gibbs free energy ΔG^0_{rxd} . At equilibrium, the concentration of all species can be expressed in the following equation:

$$K = e^{-\frac{\Delta G^0_{\text{rxd}}}{RT}} = \frac{[TP]_{\text{eq}} * [D]_{\text{eq}}}{[T]_{\text{eq}} * [DP]_{\text{eq}}}$$

For a typical reaction with an initial state $[T]_0 = 1$ nM, $[DP]_0 = 2$ nM, we let $[D] = \chi$; $[PT] = \chi$; $[DP] = (2 - \chi)$; $[T] = (1 - \chi)$. The reaction (hybridization) yield (Y) is then defined as $\chi/[T]_0$ and activation efficiency (AE) of the 3DDN is defined as $\chi/[DP]_0$. By solving the above equation using MATLAB, we are able to plot Y or AE as a function of ΔG^0_{rxd} . As an example, we detailed the MATLAB code for plotting the reaction yield and corresponding graph as following:

```

clear;clc

% For the equation of 'T + DP = TP + D', when [T]_0 = 1nM; [DP]_0 = 2nM,
% the device yield of D is calculated as below:

syms a

R = 1.987*10^-3; % kcal*K^-1*mol^-1
T = 310.15; % temperature
G = -16: 0.25: 16; % free energy range
G_d = 5.75; % free energy difference between WT and SNV_19A
yield = zeros(1, length(G));

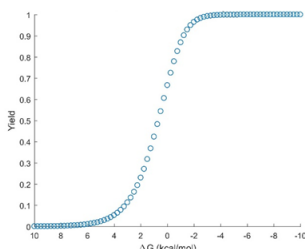
for i = 1: length(G)
    eqn = -R*T*log(a^2/((1-a)*(2-a))) == G(i);
    solx = solve(eqn, a);

    yield(i) = solx(solx>0 & solx<1);
end

scatter(G, yield);

set(gca, 'XDir', 'reverse')
xlim([-10, 10]);
title('Hybridization Yield of');
xlabel('\DeltaG (kcal/mol)');
ylabel('Yield');
legend('WT', 'Location', 'best');

```



Reaction yield and sequence selectivity as a function of ΔG^0_{rxd} . All simulation data using MATLAB were exported into Excel file for subsequent analysis. For example, the sequence analysis for 3DDN with forward toehold length (f) fixed at 9 nt and reverse toehold length (r) varying from 5 nt to 11 nt is shown in Figure S1. The reaction yield as a function of ΔG^0_{rxd} was adopted directly from the MATLAB simulation. The sequence selectivity (discrimination factor, DF) of WT over SNV19A as a function of ΔG^0_{rxd} was calculated as $DF = Y(\Delta G^0_{\text{rxd}}) / Y(\Delta G^0_{\text{rxd}} + 5.74)$. The optimal trade-off between Y and DF was achieved when $f = 10$ and $r = 10$, where $Y \approx 50\%$ (Figure 1 C & 1D).

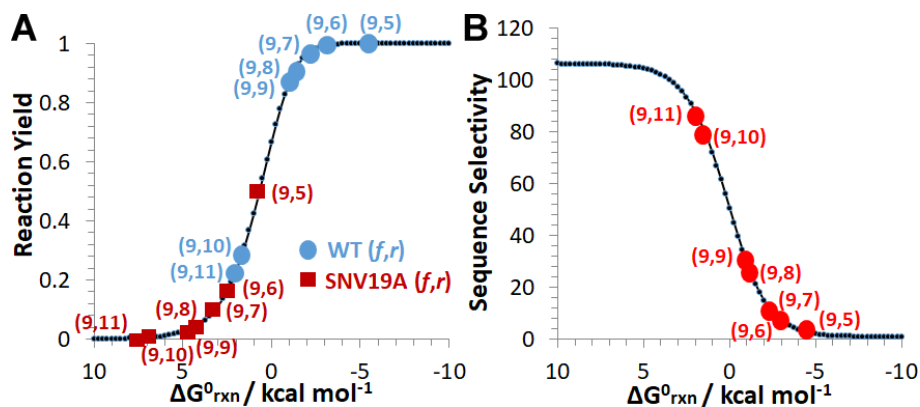


Figure S1. Simulation-guided sequence analysis for 3DDN with forward toehold length (f) fixed at 9 nt and reverse toehold length (r) varying from 5 nt to 11 nt.

Activation Efficiency as a function of ΔG^0_{rxd} . To understand how 3DDN performs throughout the concentration range in our experiment, we apply a dimensionless transformation to all DNA molecules, where a new parameter α was introduced as the ration between $[T]_0$ and $[DP]_0$. We then plotted the AE as a function of α and $[T]_0$ (Figure S2). Notably, the definition of AE ($[D]/[DP]_0$) in our system was

different from the hybridization yield (defined as $[D]/\min([T]_0, [DP]_0)$) previously described by Wu *et al.* in a similar toehold-exchange system.¹

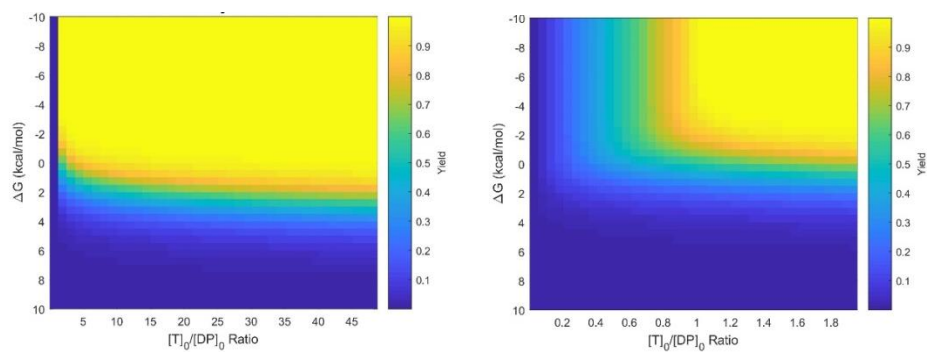


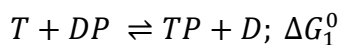
Figure S2. Activation efficiency of the 3DDN as a function of α and ΔG^0_{rxd} . The range of α in the left panel is from 0 – 50 and is 0 – 2 in the right panel.

S3. Two-Step Reaction Model and Simulation of the Non-Covalent DNA Catalysis

The non-covalent catalysis reaction can be simplified as a single overall reaction between F and DP with T serving as a catalyst:



This simplification is correct only when the intermediate TP does not accumulate significantly over the time. However, this assumption was not met in our system, as the standard free energies for all elementary reactions were very close to 0 and the intermediate TP was maintained at a non-neglectable level. We therefore simulated the non-covalent catalysis using a two-step reaction model in our system:



where $\Delta G_1^0 = \Delta G_{TP}^0 + \Delta G_D^0 - \Delta G_{DP}^0 - \Delta G_T^0$ and $\Delta G_2^0 = \Delta G_{FP}^0 + \Delta G_T^0 - \Delta G_{DP}^0 - \Delta G_F^0$. Values of ΔG_1^0 and ΔG_2^0 for WT and SNVs were calculated and listed in Table S5.

Table S5. Standard Gibbs free energies (ΔG_1^0 and ΔG_2^0) for the two-step reactions involved in the non-covalent DNA catalysis.

Sequence	ΔG_1^0	ΔG_2^0
WT	+0.98	-0.27
SNV19C	+8.42	-7.71
SNV19A	+6.72	-6.01
SNV19T	+6.47	-5.76
SNV12A	+3.98	-3.27
SNV12G	+2.92	-2.21
SNV12C	+4.41	-3.70
SNV7C	+8.30	-7.59
SNV7A	+5.99	-5.28
SNV7T	+5.61	-4.90

The equilibrium concentrations of all DNA species can then be derived by solving a set of equations:

$$K_1 = e^{\frac{-\Delta G_1}{RT}} = \frac{[D] \times [TP]}{[T] \times [DP]}$$

$$K_2 = e^{\frac{-\Delta G_2}{RT}} = \frac{[T] \times [FP]}{[F] \times [TP]}$$

After dimensionless transformation of the equations system we can introduce two tunable variables r and f and two dependent variables y and x (where $y = \frac{[D]}{[DP]_0}$, $x = \frac{[FP]}{[DP]_0}$):

$$K_1 = e^{\frac{-\Delta G_1}{RT}} = \frac{[D] \times [PT]}{[T] \times [DP]} = \frac{[D] \times ([D] - [PF])}{([T]_0 - [D] + [PF]) \times ([DP]_0 - [D])}$$

$$= \frac{[D]/[DP]_0 \times ([D] - [PF])/[DP]_0}{([T]_0 - [D] + [PF])/[DP]_0 \times ([DP]_0 - [D])/[DP]_0} = \frac{y \times (y - x)}{(r - y + x) \times (1 - y)}$$

$$\text{Similarly, } K_2 = e^{\frac{-\Delta G_2}{RT}} = \frac{x \times (r - y + x)}{(y - x) \times (f - x)}$$

By solving the two equations using MATLAB code, we were able to estimate the level of the intermediate TP (Figure S3) and the device activation efficiency (Figure S4) as a function of both $[F]_0$ and $[T]_0$ for WT and SNVs.

MATLAB Code:

```
clear; clc

% For the equation system of 'T + DP = TP + D; TP + F = FP + T', the three
% variables are "[T], [F], and [D]". And the initial state concentrations
% are [T]_0, [DP]_0 and [F]_0. For the purpose of convenience, all concentration variables can be
% dimensionlessed.

% y = [D]/[DP]_0; x = [FP]/[DP]_0; ratio = [T]_0/[DP]_0; feed = [F]_0/[DP]_0;
% these two reactions will be simplified as below:
%      y*(y-x) / ((r-y+x)*(1-y)) == K_1
%      x*(r-y+x) / ((y-x)*(f-x)) == K_2

syms x y % define a symbol used in equation

R = 1.987*10^-3; % kcal*K^-1*mol^-1
T = 310.15; % temperature
r = 0.001: 1: 50; % concentration ratio
f = 0.01: 0.2: 10; % feed ratio
G = [0.98, -0.27]; % free energy of two reactions, WT
%G = [8.42, -7.71]; % SNV 19C
%G = [6.72, -6.01]; % SNV 19A
%G = [6.47, -5.76]; % SNV 19T
%G = [3.98, -3.27]; % SNV 12A
%G = [2.92, -2.21]; % SNV 12G
%G = [4.41, -3.70]; % SNV 12C
%G = [8.30, -7.59]; % SNV 7C
%G = [5.99, -5.28]; % SNV 7A
%G = [5.61, -4.90]; % SNV 7T
effiT = zeros(length(f), length(r)); % empty matrix of device efficiency
effiF = zeros(length(f), length(r)); % empty matrix of feed efficiency

G2K = @(G) exp(-G./(R*T)); % function handle to calculate K
```

```

K = G2K(G);

for i = 1: length(f)
    for j = 1: length(r)
        % y = [D]/[DP]_0 ; x = [FP]/[DP]_0;
        eqn1 = y*(y-x) / ((r(j)-y+x)*(1-y)) == K(1);
        eqn2 = x*(r(j)-y+x) / ((y-x)*(f(i)-x)) == K(2);
        sol = vpasolve([eqn1, eqn2], [x, y]);

        effiF(i, j) = sol.x(sol.x>=0 & sol.x<min(1, f(i)));
        effiT(i, j) = sol.y(sol.y>=0 & sol.y<1);
        effiDv(i, j) = effiT(i, j)/min(1, r(j));
        effiIn(i, j) = (effiT(i, j) - effiF(i, j))/min(1, r(j));
    end
end

[X, Y] = meshgrid(r, f);
figure
m1 = pcolor(X, Y, effiT);
c1 = colorbar;
c1.Label.String = 'Yield';
caxis([0, 1]);
set(m1, 'LineStyle','none');
title('Device efficiency of Ratio and Feed, SNV 7T');
xlabel('[T]_0/[DP]_0, Ratio');
ylabel('[F]_0/[DP]_0, Feed');

figure
m2 = pcolor(X, Y, (effiT - effiF));
c2 = colorbar;
c2.Label.String = '[PT]/[DP]_0';
caxis([0, 1]);
set(m2, 'LineStyle','none');
title('Landscape of intermediate PT, SNV 7T');
xlabel('[T]_0/[DP]_0, Ratio');
ylabel('[F]_0/[DP]_0, Feed');

figure
m3 = pcolor(X, Y, effiDv);
c3 = colorbar;
c3.Label.String = 'Yield';
caxis([0, 1]);
set(m3, 'LineStyle','none');
title('Device efficiency of Ratio and Feed, SNV 7T');
xlabel('[T]_0/[DP]_0, Ratio');
ylabel('[F]_0/[DP]_0, Feed');

figure
m4 = pcolor(X, Y, effiIn);
c4 = colorbar;
c4.Label.String = '[PT]/[DP]_0';
caxis([0, 1]);
set(m4, 'LineStyle','none');
title('Landscape of intermediate PT, SNV 7T');
xlabel('[T]_0/[DP]_0, Ratio');
ylabel('[F]_0/[DP]_0, Feed');

```

Simulation Results:

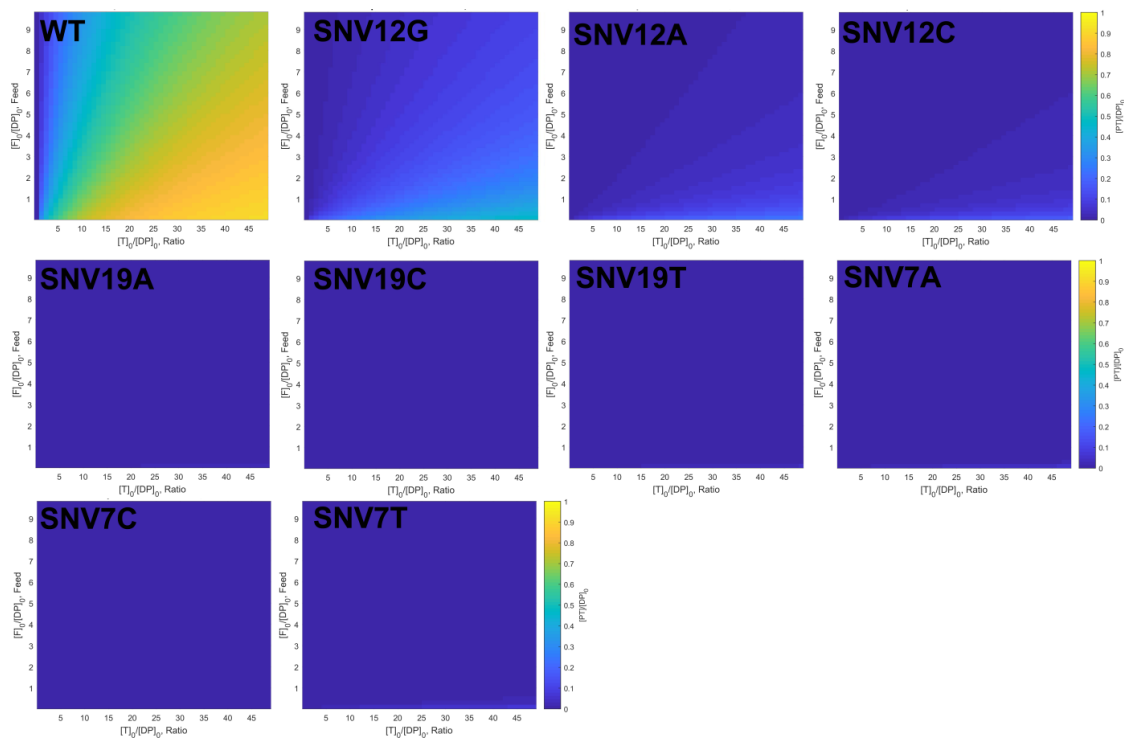


Figure S3. The level of the intermediate TP ($[TP]/[DP]_0$) as a function of $[F]_0$ and $[T]_0$.

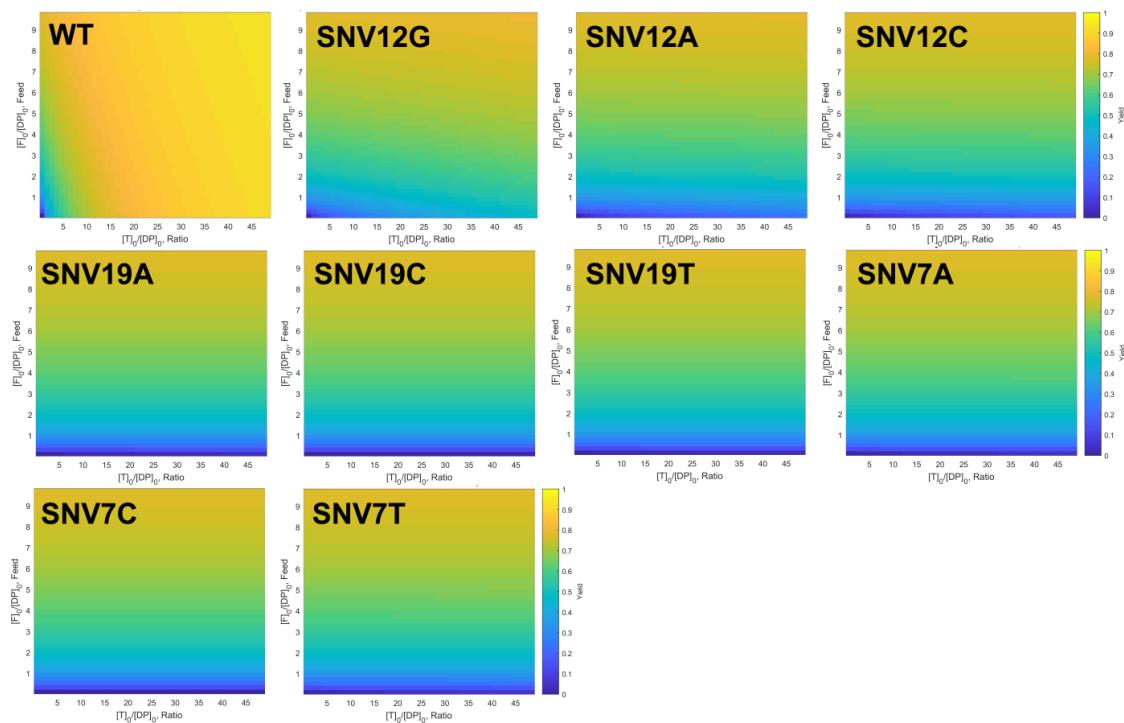


Figure S4. The device activation efficiency ($[D]/[DP]_0$) as a function of $[F]_0$ and $[T]_0$.

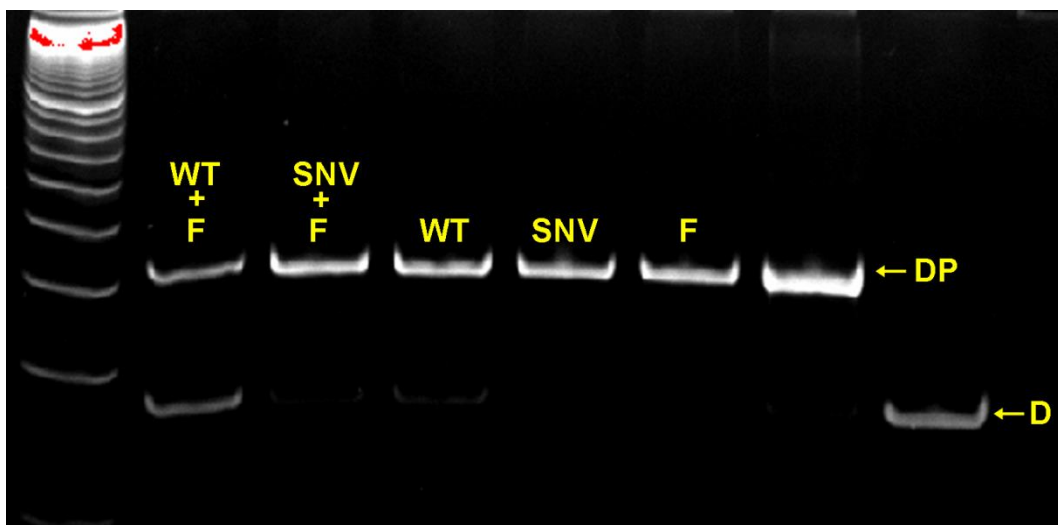


Figure S5. Characterization of non-covalent DNA catalysis for enhancing toehold exchange between T and DP using PAGE. The release of active DNA walker motif (D) could only be observed for the wild-type (WT) target (500 nM) when 2 μ M fuel (F) was added to 1 μ M DP duplex (Lane 2). This result suggests that non-covalent DNA catalysis can not only effectively enhance the assay sensitivity, but also maintain the sequence selectivity of the DNA probes.

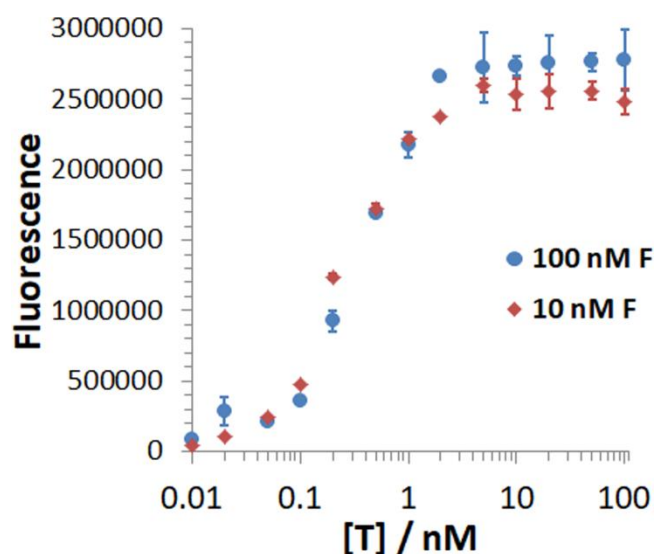


Figure S6. Experimental time-based fluorescence response (background corrected) of 100 pM 3DDN to varying concentrations of WT from 10 pM to 100 nM in the presence of 100 nM F and 10 nM F. The reaction mixtures containing varying concentrations of WT from 10 pM to 100 nM, 100 pM 3DDN, 10 nM or 100 nM F, and 20 U nicking endonuclease in $1 \times$ NEB SmartCut buffer were incubated at 37 $^{\circ}$ C for 1 hr before the fluorescence measurement. Each error bar represents one standard deviation from triplicate analyses.

S4. Prediction of the Sequence Selectivity Using $\Delta\Delta G^\circ$

It is possible to predict the reactivity of the catalytic enhanced 3DDN towards SNVs using the thermodynamic parameter $\Delta\Delta G^\circ$. We validated the $\Delta\Delta G^\circ$ -based prediction using 7 representative SNVs categorized into three groups, including those of large $\Delta\Delta G^\circ$ differences (Figure 4E), those of the same location but with different base identities (Figure S6A), and those of the same base identity at 3 different locations (Figure S6B).

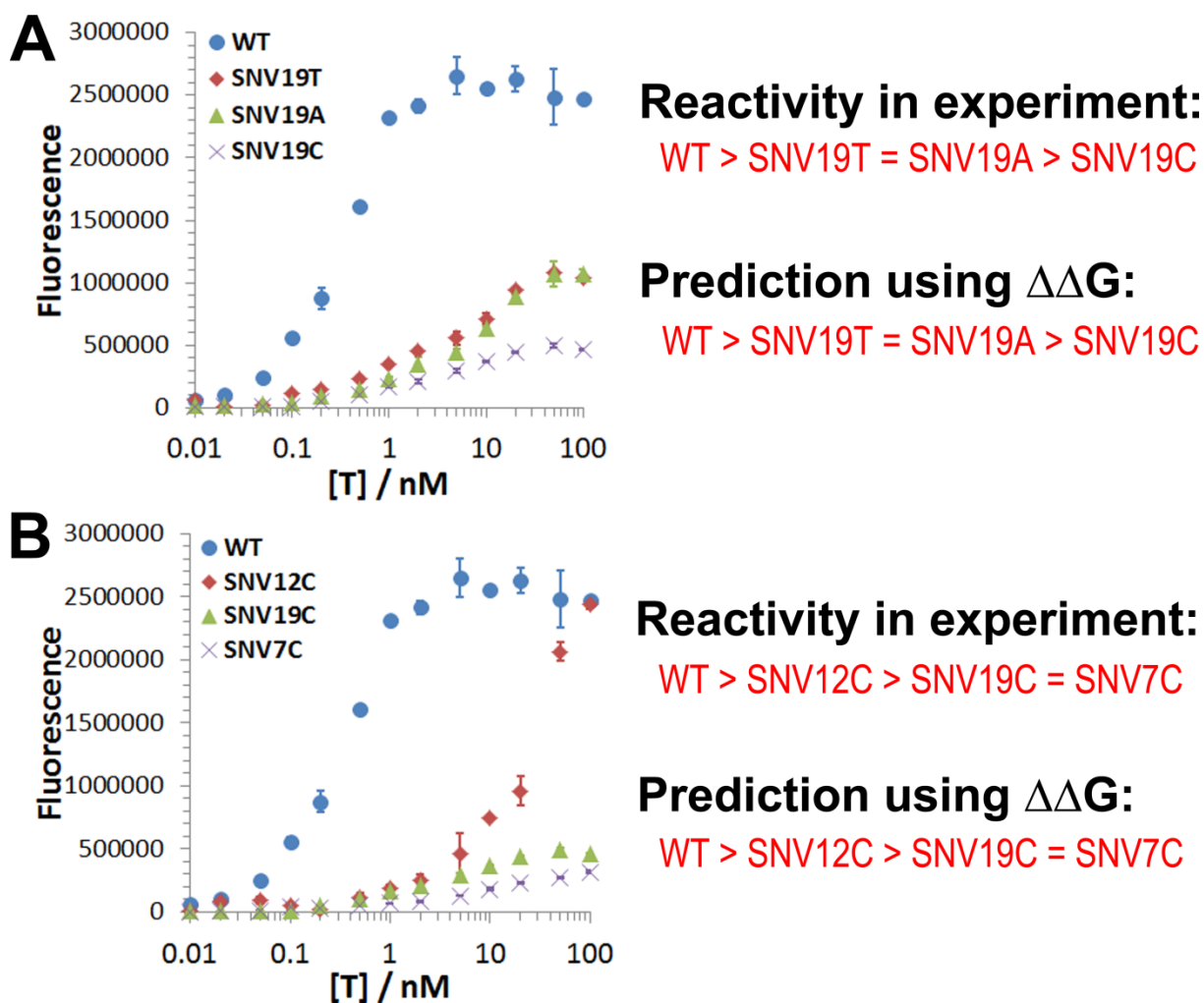


Figure S7. Validation of the sequence selectivity of catalytic 3DDN using SNVs at the same location but different base identities (**A**) and SNVs of the same base identity but different locations (**B**). The reaction mixtures containing varying concentrations of SNVs, from 10 pM to 10 μ M, 100 pM 3DDN, 10 nM F, and 20 U nicking endonuclease in $1 \times$ NEB SmartCut buffer were incubated at 37 $^\circ$ C for 1 hr before the fluorescence measurement. Each error bar represents one standard deviation from triplicate analyses.

S5. Discrimination of SNV in Complicated Sample Matrix Using Catalytic 3DDN

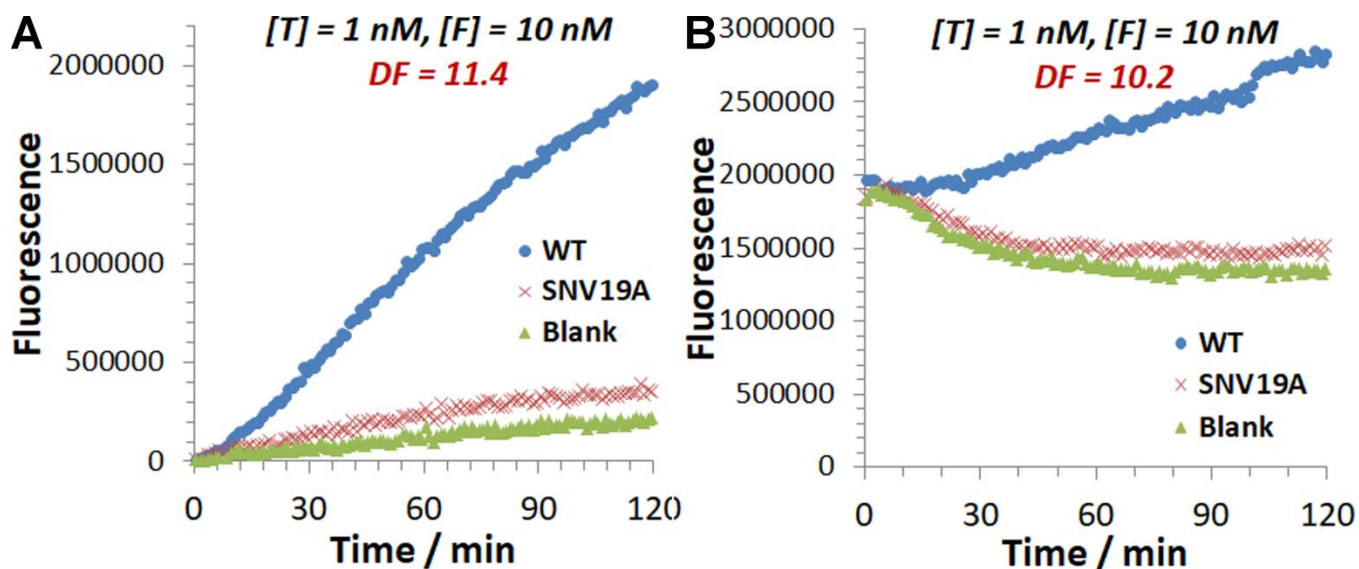


Figure S8. (A) Detection of WT and SNV19A using catalytic 3DDN in 0.1 mg/mL salmon sperm genome DNA fragments. (B) Detection of WT and SNV19A using catalytic 3DDN in 10-time diluted human serum samples. Each reaction mixture containing 1 nM WT (or SNV19A), 10 nM F, 100 pM 3DDN and 20 U nicking endonuclease in $1 \times$ NEB SmartCut buffer were incubated at 37 °C for 1 hr before the fluorescence measurement. DF was then determined using the equation that:

$DF = (F_{WT} - F_{blank}) / (F_{SNV} - F_{blank})$. Each error bar represents one standard deviation from triplicate analyses.

S6. Long-Term Stability of the 3DDN System

One important practical concern about the 3DDN system is the long-time colloidal and chemical stability of the DNA-functionalized AuNP motif. As such, we monitored the analytical performance of the same batch of 3DDN over a period of 1 month. Specifically, the activity of the active 3DDN, the stability of the inactive 3DDN (blank), and the ability to discriminate single nucleotide variation (WT against SNV19A) were measured at day 1, 3, 5, 7, 14 and 30 and plotted in Figure S9.

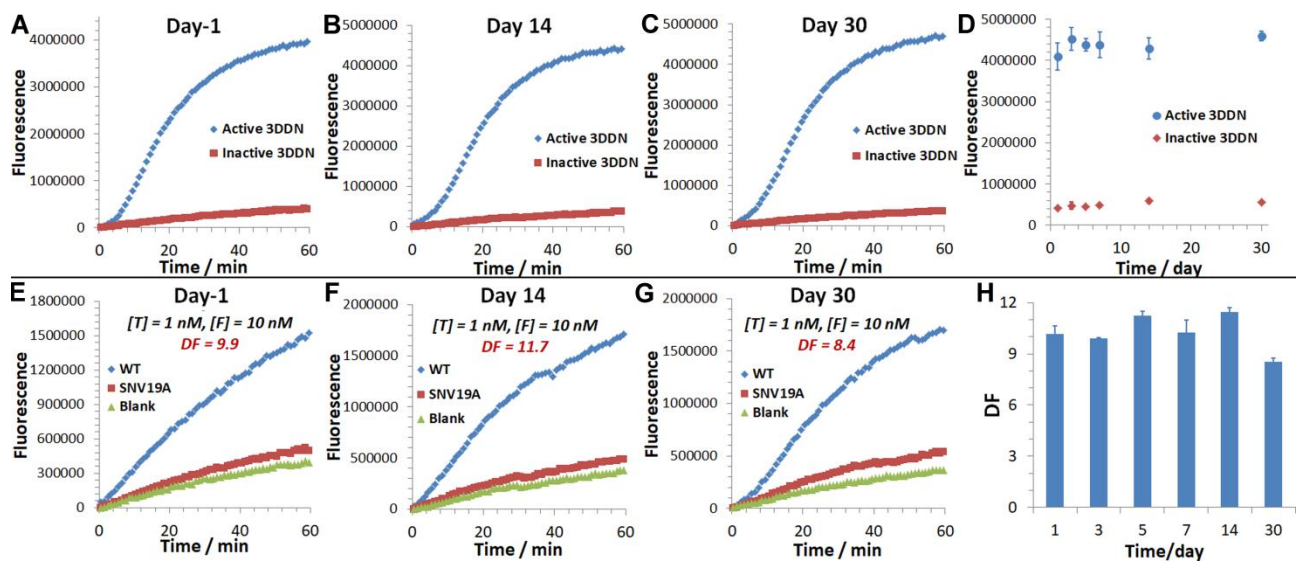


Figure S9. (A-D) Long-term activity and the chemical stability of the 3DDN system over a period of 30 days. The active 3DDN was prepared by coconjugating AuNP with R and unprotected D and the inactive 3DDN was prepared by coconjugating AuNP with R and protected D (DP). Each reaction mixture containing 100 pM 3DDN and 20 U nicking endonuclease in 1 × NEB SmartCut buffer were incubated at 37 °C for 1 hr before the fluorescence measurement. **(E-H)** Long-term activity of the 3DDN for discriminating SNVs over a period of 30 days. Each reaction mixture containing 1 nM WT (or SNV19A), 10 nM F, 100 pM 3DDN and 20 U nicking endonuclease in 1 × NEB SmartCut buffer were incubated at 37 °C for 1 hr before the fluorescence measurement. DF was then determined using the equation that:

$DF = (F_{WT} - F_{blank}) / (F_{SNV} - F_{blank})$. Each error bar represents one standard deviation from triplicate analyses.